Tailored inclusion of semiconductor nanoparticles in nanoporous polystyrene-block-polymethyl methacrylate thin films

Tailored inclusion of semiconductor nanoparticles in nanoporous polystyrene-*block*-polymethyl methacrylate thin films

Anna Malafronte,*[a] Alessandro Emendato,[a] Finizia Auriemma,*[a] Carmen Sasso,a Michele Laus,[b] Irdi Murataj,[c,d] Federico Ferrarese Lupi[c] and Claudio De Rosa[a]

a. Dipartimento di Scienze Chimiche, Università degli Studi di Napoli Federico II, Complesso Monte S. Angelo, Via Cintia, I-80126 Napoli, Italy.

b. Dipartimento di Scienze e Innovazione Tecnologica (DISIT), Università Del Piemonte Orientale A. Avogadro, Viale T. Michel 11, I-1512 Alessandria, Italy.

c. Divisione di Metrologia Dei Materiali Innovativi e Scienze Della Vita, Istituto Nazionale di Ricerca Metrologica, Strada Delle Cacce 91, 10135 Torino, Italy.

d. Dipartimento di Scienza Applicata e Tecnologia, Politecnico di Torino, Corso Duca degli Abruzzi, 24, 10129 Torino, Italy

Abstract

Nanoporous/nanocomposite thin films with controlled morphology at nanoscale were prepared onto transparent and conductive indium tin oxide (ITO) supports by exploiting the self-assembly of a lamellar polystyrene-*b*-poly (methyl methacrylate) (PS-*b*-PMMA) block copolymer (BCP). A perpendicular orientation of PS and PMMA lamellar nanodomains was achieved by grafting a random PS-*r*-PMMA copolymer to the ITO supports and successive thermal annealing. Stable and reproducible nanoporous morphologies, characterized by PS lamellar nanodomains of width equal to ≈20 nm alternating to nanochannels of width equal to ≈8 nm, were obtained by irradiating the samples with an appropriate UV-C dose able to fix the relative arrangement of PS domains through activation of cross-linking reactions and selective removal of PMMA blocks. Nanoporous hybrid composites with a stable morphology were obtained either by applying the UV irradiation protocol to BCP nanocomposites characterized by selective inclusion of zinc oxide (ZnO) nanoparticles (NPs) in the PS domains (nanocomposite first/nanopores after) or by selective infiltration of cadmium selenide (CdSe) NPs in the nanochannels left free by PMMA removal through UV irradiation (nanopores first/nanocomposite after), demonstrating the strenght of the approach.

Introduction

Surface nanopatterning with geometrical motifs having shape ranging from lamellae to cylinder or spheres of nanometric size represents one of the major story of success of polymer science and technology [1–6]. In particular, exploitation of self-assembly of block copolymers (BCPs) driven by microphase separation of incompatible blocks has been demonstrated to be a powerful tool to overcome the intrinsic limitations of conventional lithographic approches [1–9]. The shape, size and spacing of the geometrical motifs of the resultant nanostructured features may be easily controlled by the appropriate selection of blocks length, molecular mass and constitution [1–12]. A plethora of nanotechnological applications have been identified which benefit from the high versatility of BCPs to generate tailored morphologies such as separation membranes [13], tissue-

engineering [14,15], photonic crystals [16,17], as well as materials for electronic [18,19], catalysis [20], lithography [3,4,7–9], and sensing [21–24]. Furthermore, it has been shown that BCPs are ideal candidates for the fabrication of advanced nanocomposite materials through the selective inclusion of nanoparticles (NPs) with appropriate chemical affinity and geometry in specific block domains [25–33]. Indeed, nanodomains of phase-separated BCPs may act as hosts for selective inclusion of NPs, allowing for the control of nanoparticles distribution in nanocomposite thin films deposited onto solid supports. In particular, a wide range of conductive NPs, such as Au [12,18,19,22,23,28,29], Ag [18,21,25,30, 31], Pd [11] and TiO_2 [32,33], have been included in BCPs-based templates. Phase behavior, morphologies, optical and electrical properties of the obtained nanocomposites have been largely investigated as a function of nanoparticles loading [28–32], composition of block copolymers [32,34], radius and shape of nanoparticles [28,34]. The structural evolution during the application of a moving temperature gradient and the percolating behavior of the nanocomposites have been also theoretically analyzed in detail [34,35]. The simulated results demonstrated that if the loading of nanoparticles reaches a critical value termed as percolation threshold, a continuous network of nanoparticles spans the polymer host, typically leading to insulator-to-conductor transition in composites of conductive fillers and insulating host [34]. The theoretical results also reveal that the percolation threshold of nanoparticles dispersed in the block copolymers is lower than that in the host of homopolymers [34], as experimentally observed [27]. Another interesting application of self-assembling BCPs is the fabrication of materials characterized by a controlled nanoporous architecture through the selective removal of specific blocks from nanostructured BCPs [36–42]. The removal of a polymer block can be achieved by exploiting the different sensitivity of the blocks toward etching agents such as plasma, ozone, chemicals [39–41] or UV radiation [37,38], obtaining in this way nanostructured materials with well-controlled porosity, to be used for instance as photolithography masks [9], separation membranes or support for the nanoconfinement of biomolecules [40–42]. In particular, far-UV irradiation is a very common etching method able to remove and modify polymers via photo-oxidative reactions [43]. These reactions often also produce crosslinks that fix the BCP morphology making one of the blocks resistant and insoluble, thus avoiding the collapse of the structure once the other block is removed, even in severe conditions [44]. This approach is often used to obtain different nanoporous structures starting from polystyrene-*b*-poly(methyl methacrylate) (PS-*b*-PMMA) thin films thanks to the high difference in etching resistance of the blocks, as PMMA is twice more photosensitive than PS. Among the methods proposed for the selective incorporation of metal nanoparticles inside such nanoporous templates, the techniques of electrodeposition involving the motion of charged particles in solution under the influence of an electric field and subsequent deposition of the nanoparticles onto an electrode surface, have been widely investigated [26,37,45]. On the contrary, less attention has been devoted to the possibility to include NPs in the pores by using dipping procedures, simply exploiting capillary forces to sequester NPs [46]. The full exploitation of BCPs-based nanostructures and nanocomposites as functional materials in nanotechnological applications requires the control of the nanodomains orientation during the process of microphase separation. In block copolymers thin films, the interactions that are involved at polymer/support and air/polymer interfaces may strongly influence the orientation of nanodomain morphologies and the whole ordering process [47,48]. Unbalanced interactions of the blocks with the support and/or unbalanced values of surface energy at block/air interface may result in a parallel orientation of the phase separated nanodomains to the support (or air interface). Indeed, considering that the blocks are covalently linked, preferential interactions of one block with the support and/or different value of surface energy of blocks at air interface may lead to propagation of the parallel orientation of the microdomains to the support throughout the entire film thickness. The control of the orientation

of microdomains with respect to the support can be achieved adopting different strategies, namely based on the control of the interactions of the blocks at the air and support interfaces. In several nanotechnological applications, an orientation of the microdomains normal to the support is highly desired and, to this aim, the development of methods to modulate interfacial interactions is crucial [49,50]. An efficient method consists in decorating the support with a neutral layer of a random copolymer (RCP) grafted to the support. The RCP has the role to balance the interactions of each block with the support at the interface, minimizing any tendency of a block to establish preferred interactions and, as a consequence, preventing the propagation of the parallel orientation [51]. The ordering process is generally facilitated by application of suitable thermal and/or solvent vapor annealing protocols [52–54]. In particular, functional hydroxyl-terminated polystyrene-*r*-polymethylmethacrylate) (PS-*r*-PMMA) RCP grafted to the silicon surface is able to efficiently neutralize preferential interactions and to induce the perpendicular orientation in thin film of PS-*b*-PMMA BCPs [55–57]. In the present work, a symmetric PS-*b*-PMMA block copolymer sample has been used to fabricate nanoporous thin films whose polymer domains and pores have been filled with zinc oxide (ZnO) and cadmium selenide (CdSe) nanoparticles respectively, to finally obtain functional nanocomposites. The BCP films were deposited onto transparent and conductive indium tin oxide (ITO) supports. The perpendicular orientation of the BCP lamellar nanodomains was obtained by neutralizing the ITO support using a grafted layer of a PS-*r*-PMMA copolymer. The morphology of the UV-irradiated thin films was studied in detail. In particular, by means of appropriate deep UV treatments that simultaneously promote PMMA block degradation and PS block cross-linking, nanochannels of finely tunable width were obtained at the block copolymer surface with high reproducibility. The strength of the UV irradiation approach is probed in two limiting cases, by building nanoporous hybrid thin films with ZnO and CdSe nanoparticles. In particular, in the first case nanoporous nanocomposites BCP-based thin films characterized by a controlled morphology at nanometer scale were obtained by applying the UV irradiation protocol to BCP nanocomposites characterized by selective inclusion of ZnO NPs in the PS domains (nanocomposite first/nanopores after). In the second case, nanoporous nanocomposites were obtained by selective infiltration of CdSe NPs in the nanochannelsleft free by PMMA removal through UV irradiation (nanopores first/nanocomposite after). This kind of materials are extremely versatile both in composition and morphology and therefore useful for various nanotechnology applications. In particular, the designed nanocomposites, containing semiconducting NPs and prepared onto one of the most used transparent electrode (ITO) [58], can exhibit interesting properties for nanoelectronics and photovoltaic applications.

Materials and methods

Materials

Zinc acetate ($C_4H_6O_4Zn$, 99.999%, $ZnAc_2$), *ter*t-butylphosphonic acid ($C_4H_9PO_3H_2$ or TBPA, 98%), *n*-hexadecylamine ($C_{16}H_{33}NH_2$ or HDA, 98%), selenium (99.99%), cadmium chloride ($CdCl_2 \cdot 21/2\ H_2O$), 3- mercaptopropionic acid (MPA) ($C_3H_6O_2S$), hydrazine hydrate ($N_2H_4H_2O$), poly(acrylic acid) partial sodium salt solution (25 *wt*% in H_2O), carbon rods, acetic acid, methanol and toluene were purchased from Aldrich. PS-*b*-PMMA was purchased from Polymer Source, Inc. and used without further purification. The number-average molecular mass (*M*n) values of the PS and PMMA blocks in the copolymer are 25.0 and 26.0 kg mol^{-1}, respectively (polydispersity 1.06). The volume fraction of the PS block of 0.52 was selected to obtain a lamellar microphase separated morphology. The BCP sample is amorphous with glass transition temperatures equal to 108 °C for

PS and 126 °C for PMMA [59]. Indium thin oxide (ITO) coated slides (nominal transmittance >85%, nominal coating thickness of ≈130 nm) were purchased from Delta Technologies. Prior to the surface neutralization the ITO supports were sonicated in isopropyl alcohol (IPA) and subsequently in acetone for the removal of any residual organic contamination.

Neutralization of ITO supports

The supports neutralization was achieved by grafting a brush layer of ω-hydroxyl terminated poly(styrene-*r*-methyl methacrylate) (PS-*r*- PMMA) with Mn = 8.10 kg mol^{-1}, styrene fraction (f) of 58.0 (w/w) and polydispersity of 1.24. The PS-*r*-PMMA random copolymer will be indicated as "FSM6" [57]. A 9 g/L solution of FSM6 in toluene was prepared and spin-casted on the support for 60 s at 3000 rpm. The grafting process was performed by means of JetFirst 100C Jipelec rapid thermal processing (RTP) machine at 290 °C for 300 *s* [55,56]. The ungrafted random copolymer chains were subsequently removed in a sonication bath in toluene. The resulting brush layer grafted to the support was 4.5 nm [60].

Synthesis and characterization of nanoparticles

ZnO nanoparticles coated with *n*-hexadecylamine (HDA) and *tert*-butylphosphonic acid (TBPA) molecules were synthesized by thermal decomposition of $ZnAc_2$ (0.8 mmol) in hot TBPA/HDA (0.5 mmol/0.02 mol) mixture, by using the procedure described in Refs. [27, 61]. CdSe nanocrystals decorated with a hydrophilic capping (3-mercaptopropionic acid, MPA) were synthesized by an aqueous reaction of $CdCl_2$ with elemental Se in a reducing hydrazine aqueous solution mixture, by using a method previously described in Ref. [62]. Briefly, the required amount (few microliters) of MPA was added, under constant stirring, to a distilled water solution of 100 mM $CdCl_2$ up to achieve a MPA concentration equal to 0.24 M. This resulted in a clear solution. In a separate flask, the required amount of Se powder was dissolved in hydrazine hydrate (99%) in open air. Instantly the colorless solution turns dark brown and remains unchanged under atmospheric conditions at least for 2 h. In order to obtain CdSe nanoparticles of appropriate size, 100 mM water $CdCl_2$/MPA and 50 mM hydrazine hydrate-Se solutions in a volume ratio of 4:1 were mixed at room temperature and then held at 100 ◦C for 60 min to get a yellow colloid. The colloid was then precipitated by adding acetone as non solvent. The precipitate was repeatedly washed on a sintered glass filter with distilled water until its pH became normal (equal to 7). Finally, the powder was collected by drying under open-air conditions and stored in sealed bottles. The absorption spectra of the synthesized materials were recorded using a Cary Varian 5000 equipped with UV–vis monochromator, using a scanning speed equal to 50 nm min 1 and 5 nm bandwidth. UV–vis spectra of 1 mg mL^{-1} dispersions of ZnO NPs in chloroform and toluene and 0.5 mg mL^{-1} dispersions of CdSe NPs in water, dimethylformamide and ethanol were acquired. Samples for transmission electron microscopy (TEM) were prepared by casting a drop of diluted dispersions (0.5–1 mg mL^{-1}) of ZnO and CdSe NPs in toluene and ethanol, respectively, on the surface of a carbon-coated copper grid. Powder wide-angle X-ray diffraction (WAXS) profiles were obtained with Ni-filtered Cu Kα radiation using an Empyrean diffractometer by PANalytical with continuous scans of the 2θ angle and a scanning rate of 0.02°/s. The diameters (d) of ZnO and CdSe NPs were estimated by using the Sherrer formula (Equation (1)):

$$d = K\lambda/(\beta \cos \vartheta)$$

where *d* is the mean crystallite diameter, *K* is a shape factor set equal to 0.9 rad, λ is the X-ray wavelength, β is the width at half height (FWHM) of intensity for the most pronounced 100 reflection of ZnO wurzite crystal at 2θ ≈ 31.1° and 111 reflection of CdSe cubic crystals at 2θ ≈ 25.3°. No correction for the instrumental line broadening was performed, due to the high broadness of the Bragg peaks of both ZnO and CdSe nanocrystals.

Neat BCP thin films preparation

The PS-*b*-PMMA thin films (thickness ≈ 70 nm) were prepared by spin coating (3000 rpm for 30 s) 1 wt% BCP solutions in toluene onto FSM6-ITO supports. The solutions were previously stirred for 4 h at 50 °C to ensure complete BCP dissolution. Thermal annealing procedure was performed by placing the thin films in a vacuum oven at 190 °C for 24 h. The PMMA etching was performed by irradiating the thin films with 254 nm UV-C radiation using a Spectroline ENF-240c/FE 4 W portable lamp. Samples were placed 9 cm away from the UV source and treated for different irradiation times (15, 45, 60, 90 and 120 min) in order to study the effect of this treatment on the morphology of the samples. After the irradiation, the samples were dipped into glacial acetic acid for 30 min to remove fragments derived from the etching process, and then dried under fume hood. The effective irradiance sustained by the samples was measured using a DeltaOhm HD2102.1 photoradiometer equipped with a LP471UVC probe and calibrated against a 254 nm filtered mercury lamp.

Preparation of nanocomposites of ZnO NPs

Toluene solutions containing the PS-*b*-PMMA BCP (1 wt %) and ZnO NPs (0.1 wt%) were prepared and vigorously stirred for 24 h. Thin films were obtained by spin coating (3000 rpm for 30 s) the toluene solutions onto FSM6-ITO supports at room temperature. Subsequently, the nanocomposite thin films were annealed in vacuum at 190 °C per 24 h. The PMMA blocks were removed from the nanocomposites by irradiating the thin films with 254 nm UV-C radiation adopting the best procedure identified for the neat thin film, that is using an irradiation time of 60 min, placing the samples 9 cm away from the UV source.

Preparation of nanocomposites of CdSe NPs

CdSe nanoparticles were included in the BCP nanoporous thin films by using dipping procedures. In particular, the BCP nanoporous samples were immersed in a 0.5 mg mL^{-1} CdSe dispersion in ethanol and withdrawn normal to the dispersion surface. The immersion and reemergence rates were fixed to 6 cm/min and controlled by means of a mechanical arm. Different experiments were performed varying the number of immersion/reemergence cycle (1, 3, 6, 10) and the sample/ NPs dispersion contact time for each cycle (900, 300, 150, 90 s), for a total contact time equal to 900 s in every experiment. The CdSe dispersion was kept under vigorous stirring during the dipping procedure. The solution excess was removed from the surface of the films with a filter paper and successive drying the samples under a fume hood. The solution excess was removed from the surface of the films with a filter paper and drying the samples under a fume hood.

Microscopy characterization

TEM images were obtained in bright field mode using a FEI Tecnai G2 200 kV Transmission Electron Microscope with an accelerating voltage of 120 kV and 200 kV. The thin films were coated with carbon by using the Emitech K950X turbo evaporator. Carbon rods were mounted in the vacuum system (5×10^{-5} mbar) between two high-current electrical terminals and heated to their evaporation temperature, allowing the deposition of a fine stream of carbon (thickness 3–4 nm) onto specimens. Then, drops of poly(acrylic acid) partial sodium salt solution (25 wt % in H_2O) were deposited on the surface of the carbon-coated films and the samples were dried under a fume hood overnight. Dried drops consisting of polymeric thin films backed with carbon lying onto a dried poly(acrylic acid) support were removed from the support with a knife. Poly(acrylic acid) was dissolved by floating the dried drops onto water (with the poly(acrylic acid) at the interface with water), and finally, the carbon-coated polymers were recovered by fishing onto a 200 mesh TEM copper grid. In order to achieve a good contrast between the different BCP domains, some films were stained with RuO_4 by exposition of the TEM grids to RuO_4 vapors for 40 min at room temperature. TEM analysis was repeated for different regions of the specimen to check the uniformity of the morphology over the macroscopic area of the support and for independent samples. The size of the NPs and the average width of the PS and PMMA lamellar nanodomains and of the nanochannels were calculated from the TEM images using ImageJ software (National Institutes of Health, available free of charge at Web site rsb.info.nih.gov/ij/). At least 200 independent measurements were taken at different locations of the TEM images of the samples. The measurements were also confirmed by repeating the analysis on TEM images of independent samples. Scanning electron microscopy (SEM) micrographs were collected using a FEG Inspect-F FEI system at 30 kV, with a spot of 3.0 and working distance of 10 mm. Atomic force microscopy (AFM) measurements were carried on a Bruker Multimode 8, in Bruker peakforceTM mode, using an antimony-doped silicon cantilevers RTESPA-300 tip with radius of about 8 nm, at resonance frequency and force constant of about 300 kHz and 40 N/m, respectively. No touch tip calibration was performed before every observation. Images were recorded at room temperature at 0.5 Hz scan rate, 1 kHz frequency and 150 nm amplitude; the peakforce setpoint and gain were optimized for each image to improve quality. Several positions for each sample were scanned to ensure consistency among the observations. The size of the scans was equal to 1 × 1 µm. The height profiles were extracted from the AFM images using Gwyddion software (http://gwyddion.net).

Results and discussion

Fabrication of the BCP-based nanoporous material with controlled morphology at nanometer scale

The first step of this work consisted in setting up a robust and reproducible procedure to obtain nanostructured thin films of a symmetric diblock copolymer PS-*b*-PMMA (25 kDa–26 kDa), onto Indium Tin Oxide (ITO) supports, characterized by a perpendicular orientation of the lamellar PS and PMMA nanodomains. After neutralization of the ITO support with a grafted random PS-*r*-PMMA copolymer (named FSM6), BCP thin-films were prepared by spin coating and successively subjected to thermal annealing treatments in order to provide sufficient mobility to the polymer chains and achieve a perpendicular orientation of the PS and PMMA lamellar domains. A representative TEM image of BCP thin films deposited onto an ITO support functionalized with the random copolymer FSM6 (ITO-FSM6 support), after thermal annealing at 190 °C for 24 h, is

reported in Fig. 1A. The dark regions correspond to the RuO4-stained PS lamellar nanodomains, whereas the PMMA domains appear bright in the images. The results indicate the obtainment of a well oriented perpendicular lamellar morphology (Fig. 1A). The average lamellar widths evaluated from the image of Fig. 1A are ≈19 ± 2 and ≈9 ± 1 nm for PS and PMMA, respectively. The PS-*b*-PMMA thin films deposited onto FSM6-ITO supports by spin-coating and annealed at 190 °C for 24 h (Fig. 1A) were exposed to deep UV-C irradiation for different amounts of time using a mercury UV lamp with maximum emission at 254 nm.

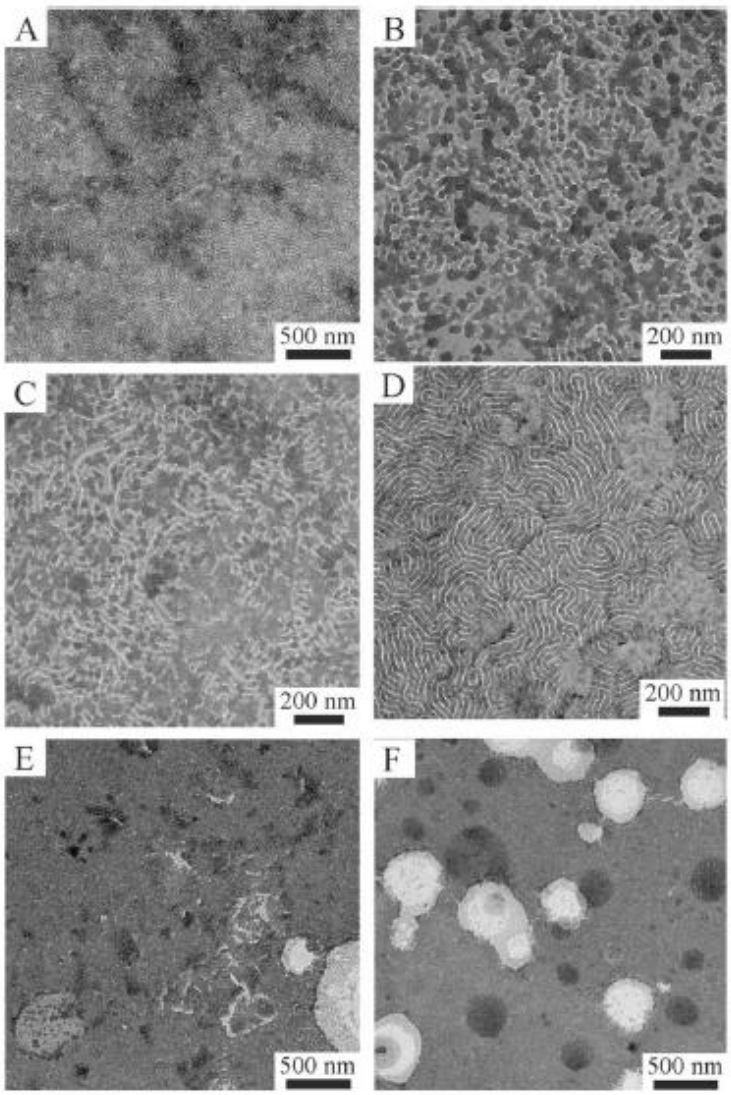

Fig. 1. Bright-field TEM images of PS-*b*-PMMA thin films, prepared by spin coating toluene solutions of 1 wt% BCP onto FSM6-ITO supports and annealed at 190 °C for 24 h, after different UV irradiation times of 0 (A), 15 (B), 45 (C), 60 (D), 90 (E) and 120 (F) min and washing with acetic acid. Staining with RuO4 was performed before TEM observation.

Depending on dose and experimental conditions, UV irradiation is expected to induce rapid degradation of PMMA blocks, and slow degradation, eventually coupled with occurrence of cross-linking reactions, of PS domains [44,63]. The exact mechanism involving PS chains is still unclear. It has been suggested that in presence of oxygen, proton abstraction can be followed by addition of an oxygen molecule, and consequent generation of radical species that can either react with another polymer chain forming an oxygen bridge, or undergo β-scission reactions leading to PS degradation [43,44]. The TEM images of PS-*b*-PMMA thin films, deposited onto FSM6-ITO supports

and annealed at 190 °C for 24 h, after exposure to UV irradiation for different times and dipping into glacial acetic acid for 30 min to remove fragments derived from the etching process, are shown in Fig. 1B–F. The morphologies of the untreated sample (Fig. 1A) and of the samples irradiated for 15 and 60 min (Fig. 1B and D, respectively) were also confirmed by SEM analysis (Figure S1). As discussed before, the untreated sample (Fig. 1A) shows a lamellar morphology characterized by PS and PMMA lamellar widths equal to ≈ 19 nm and ≈9 nm, respectively. After 15 min of irradiation time (irradiation dose of 155 mJ/cm^2) and successive acetic acid washing (Fig. 1B) the morphology is impaired, and only few regions are left decorated with striped motifs reminiscent of the initial nanostructure. On the contrary, as a result of irradiation for 45 and 60 min (energy dose of 465 mJ/cm^2 and 630 mJ/ cm^2 respectively), the lamellar morphology of the BCP thin film resembles the pristine one (Fig. 1C and D). This indicates that for irradiation times higher than 15 min, the cross-linking reactions of PS are enough to allow for PMMA removal while maintaining the lamellar morphology (Fig. 1C and D). This is particularly evident for irradiation time of 60 min (Fig. 1D) where the PS cross-linking fixes and stabilizes the lamellar morphology of the initial BCP nanostructure (Fig. 1A), resulting in the formation of well-defined nanochannels alternating to the residual PS cross-linked lamellar domains (Fig. 1D). However, after 90 min of irradiation time (Fig. 1E) only few lamellae survived to the treatment and after 120 min (Fig. 1F) the copolymer morphology is completely lost. These results suggest that an irradiation time longer than 60 min (Fig. 1 E, F) resulted in an almost complete deterioration of the BCP morphology. The size of the PS nanodomains and PMMA/nanochannels obtained after different irradiation times (comprised between 0 and 60 min), evaluated from the TEM images of Fig. 1A–D, are reported in Fig. 2. It is apparent that the spacings of the lamellar morphology significantly change during the UV treatment. After 15 min UV irradiation (Fig. 1B), the polymeric lamellar domains left attached to the support (dark regions in the TEM image) exhibit an increase of the width from ≈19 nm to ≈ 23 nm. These domains alternate to nanochannels with average width of only ≈4 nm. The value of the channel width of ≈4 nm is lower than the average width of the PMMA lamellar domains in the initial untreated sample (≈9 nm, Fig. 2).

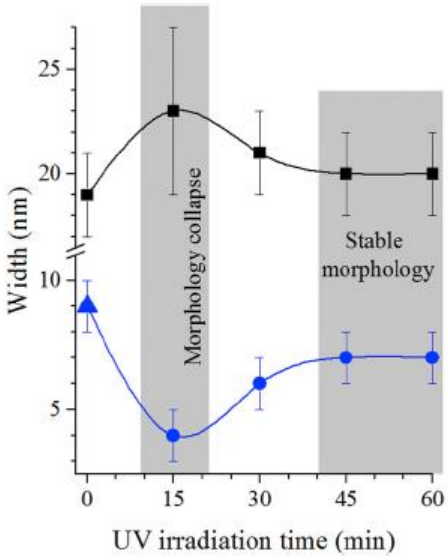

Fig. 2. Size of the PS nanodomains (black squares) and of nanochannels (blue circles) left free upon removal of PMMA blocks after UV irradiation for 15, 30, 45 and 60 min. The blue triangle indicates the width of PMMA domains before UV irradiation (zero irradiation time). Nanochannels were obtained after UV irradiation of PS-*b*-PMMA thin films, prepared by spin coating toluene solutions of 1 wt% BCP onto FSM6-ITO supports and annealed at 190 °C for 24 h, for different times (15, 30, 45 and 60 min). (For interpretation of the references to color in this figure legend, the reader is referred to the Web version of this article.)

The decrease of the channel size and the increase of the width of dark domains may either due to the collapse of adjacent PS domains into a single domain of higher lateral size, or to a partial degradation of PMMA. In this second hypothesis, oxidation reactions of PS covalently linked to shorter PMMA moieties surviving onto ITO/FSM6 support give rise to elongated domains, able to adsorb similar amount of the staining agent, so that the apparent width of domain size increases from 19 to 23 nm. This second hypothesis is based on the observation that the center-to-center distance between consecutive PS domains does not change within the experimental error with increasing the UV irradiation time. In the first hypothesis, indeed, a doubling of the width of the PS domains would be observed. By increasing the UV irradiation time, the width of the channels gradually increases whereas the width of the polymeric domains decreases. In particular, after 45 and 60 min of UV irradiation (Fig. 1C and D), the width of the dark lamellar nanodomains (≈19 ± 2 nm) is the same of the PS domains in the untreated sample (20 ± 2 nm). These domains alternate with nanochannels of width equal to 8 ± 1 nm (Fig. 2), confirming that both complete PMMA degradation and efficient PS crosslink, able to fix the initial BCP morphology, occurred. The selective degradation of the PMMA blocks was confirmed by AFM analysis (Fig. 3).

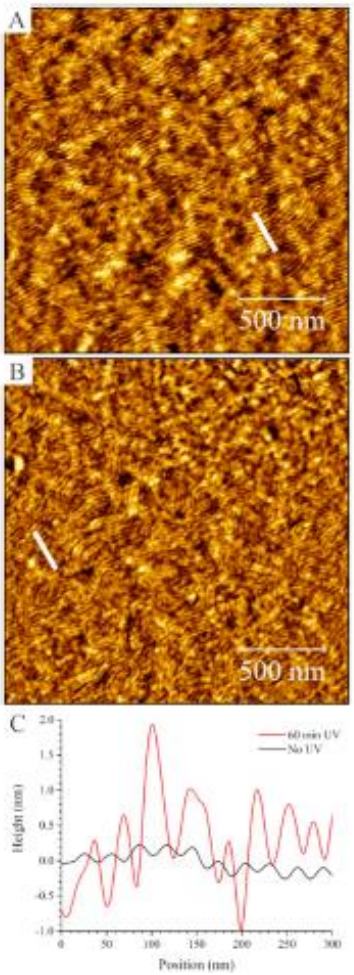

Fig. 3. AFM height images of PS-*b*-PMMA thin films, prepared by spin coating toluene solutions of 1 wt% BCP onto ITO-FSM6 supports after thermal annealing at 190 °C for 24 h, before (A) and after (B) 60 min of UV irradiation. Height profiles extracted from the AFM micrographs are reported in C.

The untreated sample PS-*b*-PMMA, prepared onto ITO-FSM6 support after thermal annealing at 190 °C for 24 h, shows an ordered lamellar morphology (Fig. 3A) with only a small difference in height between the two blocks (Fig. 3C). On the other hand, for the 60 min UV-irradiated sample (Fig. 3B), a significant difference in height between the two blocks was found (Fig. 3C). Indeed, as shown by the height profiles extracted from the AFM images (Fig. 3C), undulations with amplitude lower than ≈ 0.2 nm and higher than ≈ 1.5–2 nm occur for the samples before and after UV irradiation, respectively, confirming the selective removal of the PMMA blocks. The width of the surviving PS domains and nanochannels are ≈19 nm and ≈9 nm, respectively, in agreement with the values extracted from TEM analysis (Fig. 2). AFM images of the 15 and 45 min UV-irradiated samples are reported in Figure S2. The channels are not visible in the Figure S2A, since for the 15 min UV-irradiated thin film the width of the channels (≈4 nm, Figs. 1B and 2) is lower than the radius of the used AFM tip (tip radius ≈ 8 nm). Featureless regions alternating with regions presenting channels having a width equal to ≈9 nm, alternating to PS lamellar domains of width ≈19 nm, are instead observed in the case of the 45 min UV-irradiated sample (Figure S2B), in agreement with the TEM analysis (Figs. 1C and 2). The samples after 15 and 60 min of UV treatment (Fig. 1B and D, respectively) were immersed for 120 min in toluene in order to probe the effective occurrence of crosslinking reactions of PS domains (Fig. 4).

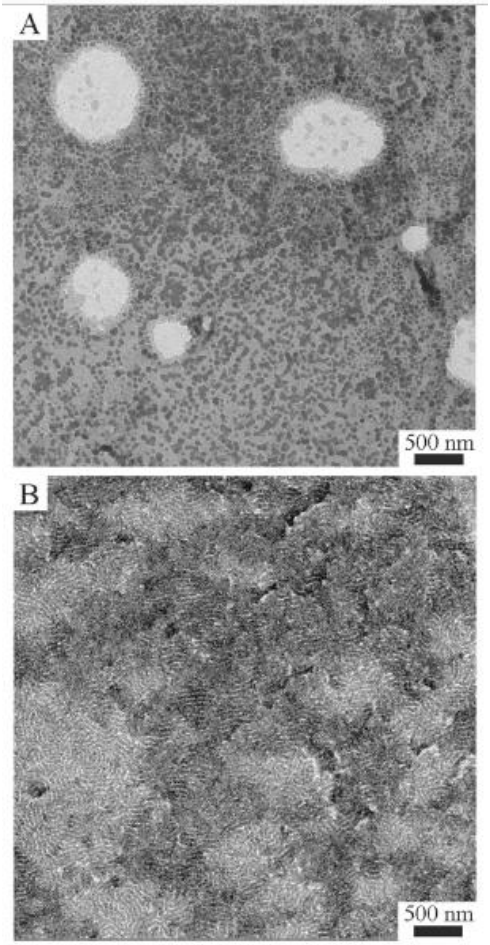

Fig. 4. Bright-field TEM images obtained after immersion in toluene for 120 min of the 15 min (A) and 60 min (B) UV-irradiated PS-*b*-PMMA thin films, prepared by spin coating toluene solutions of 1 wt% BCP onto FSM6-ITO supports and annealed at 190 °C for 24 h. Staining with RuO_4 was performed before TEM observation.

Polystyrene, in fact, becomes insoluble in this solvent by effect of crosslinking [37]. It is apparent from the TEM images of Fig. 4 that, after toluene immersion, the initial morphology of the 60 min UV-treated sample (Fig. 1D) is retained even after 120 min immersion in toluene (Fig. 4B), indicating that the cross-linked PS blocks stick firmly to the support, fixing the final nanoporous morphology. Instead, in the case of the 15 min UV-treated sample (Fig. 1B), (or non UV irradiated film, data not shown), the immersion in toluene causes almost complete destruction of the initial morphology due to partial dissolution of the film in the solvent (Fig. 4A).

Synthesis and characterization of ZnO and CdSe NPs

Semiconductor ZnO NPs capped with *n*-hexadecylamine (HDA) and *tert*-butylphosphonic acid (TBPA) were synthetized by using the procedure described in References 27 and 54. The wide angle X-ray powder diffraction (WAXS) profile, TEM image and UV–Vis absorption spectra of the obtained ZnO NPs are reported in Fig. 5A, A′ and A′′, respectively. The broad diffraction peaks present in the WAXS profile of the ZnO nanoparticles suggest a wurtzite structure [54] and a value of the mean crystallite diameter (*d*), evaluated by using Equation (1) (Experimental Section), equal to 5.3 nm. The dimension of the ZnO nanoparticles was confirmed by TEM analysis from which a value of the average NPs diameter equal to 5.7 ± 0.9 nm was determined. The UV–Vis spectra of ZnO NPs (Fig. 5 A′′) show a quite steep onset and a maximum absorption at 332 nm, both in chloroform (curve a of Fig. 5 A′′) and toluene (curve b of Fig. 5 A′′). CdSe nanoparticles decorated with a hydrophilic capping (3-mercaptopropionic acid, MPA) were synthetized according to the method of Ref. 55. The capping molecules help controlling the nanometric size of CdSe crystals limiting crystal growth through Ostwald ripening phenomena and at the same time help achieving an efficient dispersion of the NPs in an orthogonal solvent (namely ethanol) to the BCP PS domains. The WAXS profile of the CdSe NPs (Fig. 5B) shows two broad humps at the positions $2\theta \approx 25.3°$ and ≈44.8° of the 111 and 220 + 311 reflections of the cubic zinc-blend-like structure of CdSe [64]. The correlation length of the crystals in the direction normal to (111) planes, estimated from the width at mid-height of the hump at $2\theta \approx 25.3°$, by using the Sherrer's equation (Equation (1), Experimental Section), is equal to ≈ 3.2 nm. The TEM image of the CdSe NPs (Fig. 5B′) shows well-separated nanoparticles of average diameter equal to 3.3 ± 0.9 nm, in agreement with the results of diffraction analysis. The small size of CdSe NPs is also confirmed by the UV absorption spectra recorded in different hydrophilic media (Fig. 5B′′). They show a strongly blue shifted absorption edge at 390 nm with respect to the CdSe bulk edge at 713 nm [65], due to a quantum confinement effect.

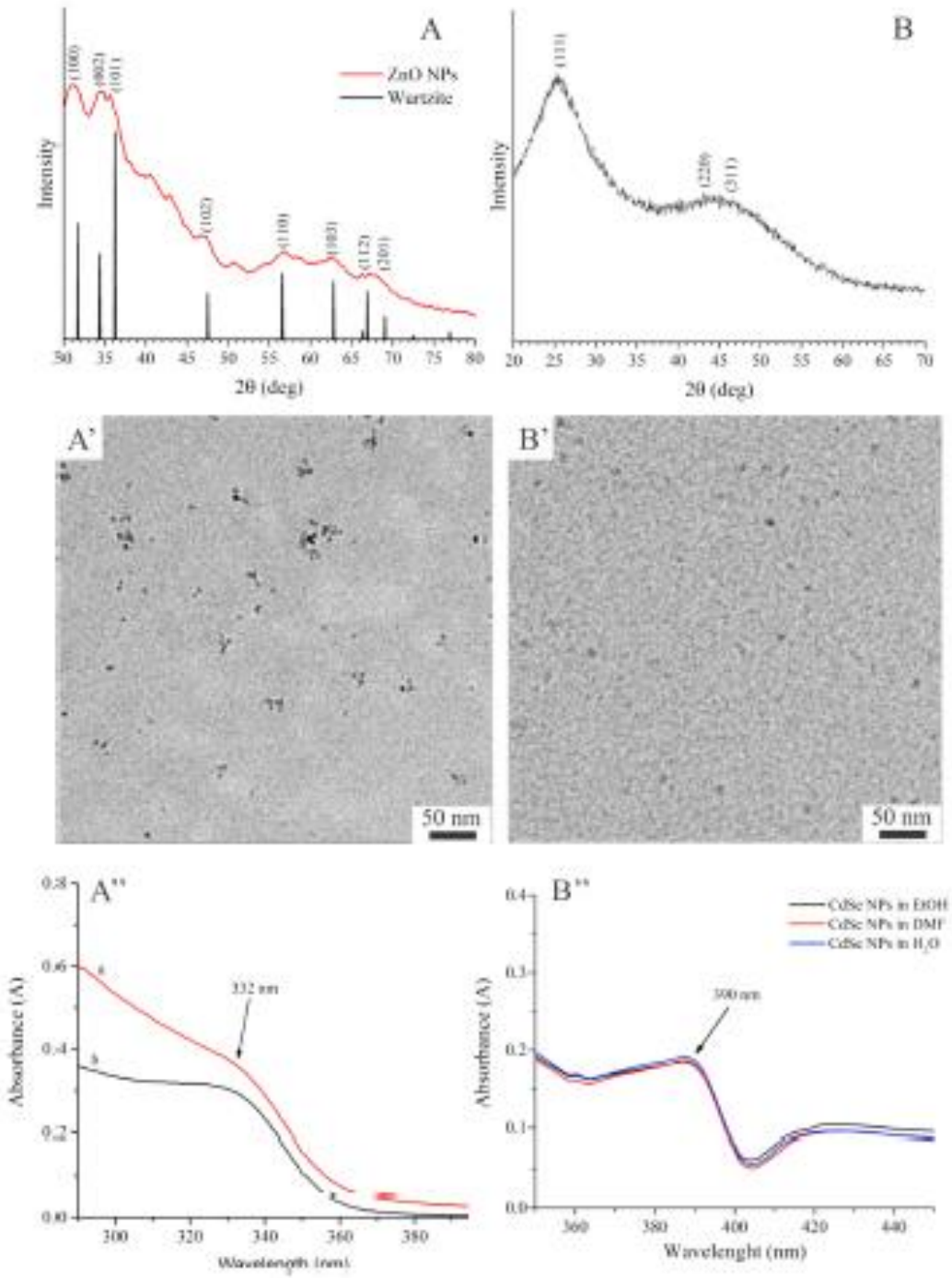

Fig. 5. Wide angle X-ray powder diffraction (WAXS) profiles (A, B), bright-field TEM images (A' , B') and UV–Vis absorption spectra in different solvents (A'', B'') of synthetized organic capped ZnO (A-A'') and CdSe (B-B'') nanoparticles. The *hkl* Miller indices of the main reflections of ZnO wurtzite structure and CdSe cubic zinc-blend-like structure are indicated in A and B, respectively. UV–Vis spectra were acquired by dispersing the ZnO NPs in chloroform and toluene (curve a and b in A'', respectively) and by dispersing CdSe NPs in ethanol (EtOH), dimethylformamide (DMF) and water (black, red and blue line in B'', respectively). (For interpretation of the references to color in this figure legend, the reader is referred to the Web version of this article.)

Fabrication of the BCP-based nanoporous nanocomposites

Nanoporous nanocomposites were prepared by selective inclusion of the semiconductor ZnO NPs, capped with a mixture of TBPA/HDA in the PS nanodomains and successive PMMA removal by UV-

C irradiation (nanocomposite first/nanopores after), and by infiltering CdSe NPs, capped with hydrophilic MPA, in the nanochannels of the nanoporous BCP films (nanopores first/nanocomposite after).

ZnO-based nanoporous nanocomposites (nanocomposite first/ nanopores after)

ZnO NPs were included in the PS lamellar domains of the BCP by dispersing the NPs and BCP in a common solvent (toluene), successive preparation of the thin films and subsequent thermal and UV treatments. The best results were obtained adopting 60 min irradiation time with the UV-C lamp, in agreement with the protocol identified for the neat BCP (Fig. 1D). The TEM images of the nanocomposite containing ZnO NPs, before and after the PMMA removal, are reported in Fig. 6 A, A' and B, respectively. The images of the PS-*b*-PMMA/ZnO NPs nanocomposite (Fig. 6A, A') indicate the selective inclusion of the NPs in the lamellar RuO4-stained PS nanodomains. The nanoparticles filling the PS blocks are clearly visible in the high magnification inset of the nanocomposite reported in Fig. 6A'. Interestingly, the UV treatment of the PS-*b*-PMMA/ ZnO NPs nanocomposite does not alter neither the morphology nor the localization of the ZnO NPs (Fig. 6B), allowing the obtainment of nanoporous thin films consisting of PS lamellar nanodomains filled with ZnO NPs alternating to nanochannels left after PMMA removal by UV treatment. It is worth to note that in this case, due to the absence of PMMA blocks, a good contrast in the TEM image is obtained without resorting to any staining procedure (Fig. 6B).

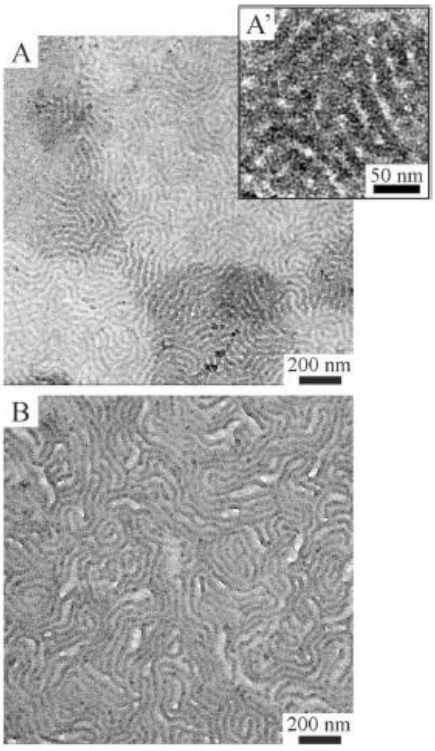

Fig. 6. Bright-field TEM images of thin films prepared by spin-coating toluene solutions containing PS-*b*-PMMA BCP and ZnO NPs onto FSM6-ITO supports, and annealed at 190 °C for 24 h, before (A, A') and after (B) UV treatment for 60 min. The image A and A' were acquired after RuO4 staining; no staining procedure, instead, was performed onto the UV-treated sample (B).

CdSe-based nanoporous nanocomposite (nanopores first/ nanocomposite after)

Selective inclusion of CdSe nanoparticles in the nanochannels of the BCP-based porous template was achieved by dipping the nanoporous BCP thin films (60 min UV irradiation, Fig. 1D) into an ethanol dispersion of CdSe NPs and successive withdrawing of the films in the direction normal to the dispersion surface, using the procedure described in the experimental section. Representative TEM images of the cycles and by using a sample/NPs dispersion contact time for each cycle equal to 150 s are shown in Fig. 7, before (Fig. 7A) and after (Fig. 7B, B') RuO_4 staining procedure. The presence of CdSe NPs and nanochannels allows the detection of the lamellar morphology without any staining procedure in Fig. 7A. Upon RuO_4 staining (Fig. 7B, B'), a clear contrast difference between the PS lamellae of the BCP and the nanochannels is evidenced.

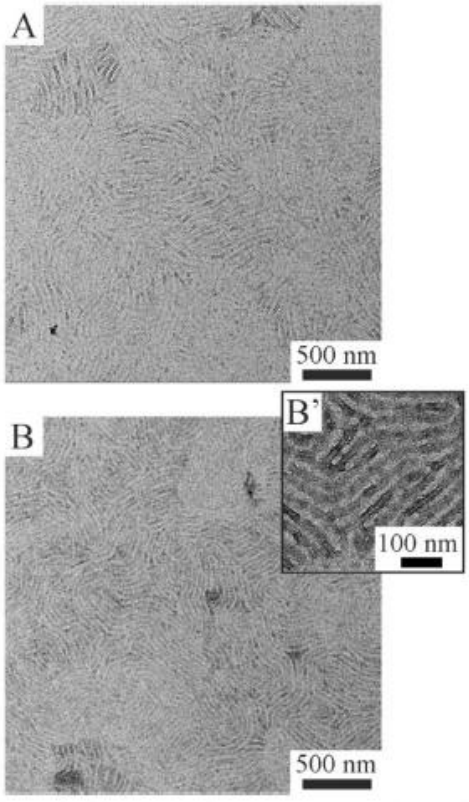

Fig. 7. Bright-field TEM images of nanoporous/nanocomposite thin films obtained by dipping the BCP-based nanoporous thin film in the CdSe NPs ethanol dispersion before (A) and after (B, B') RuO_4 staining of the PS domain. Six immersion/reemergence cycles and a sample/NPs dispersion contact time for each cycle equal to 150 s were used.

The images show that CdSe NPs are mainly localized at the interface between the nanochannels and the PS lamellar domains. Due to the small dimensions of the CdSe NPs (≈3 nm), the nanoparticles appear as dark continuous rows in the high magnification inset of the TEM image of the nanocomposite (Fig. 7B'). The sequestration of the NPs is due to the capillary forces acting on the dispersion upon normal withdrawal of the porous template. We found that a number of immersion/reemergence cycles of about 6 was enough to obtain a good nanoporous morphology characterized by selective inclusion of the nanoparticles in the channels. A too high number of cycles resulted, however, detrimental for the BCP nanoporous morphology (data not shown), due to the intrinsic tendency of NPs to aggregate. The comparison between the TEM images of the nanoporous nanocomposites thin films acquired without resorting to any staining procedure (Figs.

6B and 7A) clearly confirms the different location of the ZnO and CdSe NPs in the nanoporous template. PS lamellar nanodomains, in fact, appear dark in the TEM image of Fig. 6B because they are filled with ZnO NPs. On the contrary, the unfilled PS nanodomains appear bright in the case of the nanocomposites containing the CdSe NPs (Fig. 7A). The developed two-step strategy paves the way to the fabrication of more complex, multicomponent systems in which the positioning of different nanoparticles can be simultaneously controlled at nanometer scale. In addition, the use of a self-assembled BCP as template for the NPs inclusion allows obtaining a high interface between the two included NPs, beneficial for a plethora of nanotechnological application. In particular, in Ref. 27, it has been already demonstrated that hybrid nanocomposites characterized by the selective inclusion of ZnO NPs in the PS lamellar domains of PS-*b*-PMMA BCP thin films, show good electrical conductive properties before PMMA removal, provided that the ZnO NPs content is above a threshold concentration [27,34]. Such good electrical conductive properties are expected also for the nanoporous BCP thin films obtained after selective removal of PMMA blocks. Furthermore, possible applications suitable for exploitation of the simultaneous inclusion of NPs with opposite charge carrier ability in adjacent domains may be also envisaged in the fabrication of electro-optical devices, the performances of which are critically dependent on the charge transfer efficiency at the interfaces, coupled with carrier ability of the opposite charges along well-separated paths, in order to reduce to a minimum charge recombination.

Conclusions

A robust experimental procedure to fabricate nanoporous nanocomposite thin films, based on PS-*b*-PMMA BCP, onto conductive and transparent ITO supports was set up. Thin films, characterized by a perpendicular orientation of PS and PMMA lamellar nanodomains, were obtained by using ITO supports functionalized with a random PS-*r*- PMMA copolymer coupled with thermal annealing at 190 °C for 24. Appropriate UV-C irradiation of the so obtained thin films selectively removes the PMMA blocks, allowing the formation of nanochannels on the block copolymer surface. The preservation of the pristine morphology of the porous material was achieved by selecting the UV-irradiation conditions able to induce the simultaneous PMMA degradation and cross-linking of PS domains. In this case, nanochannels having the same width (≈8 ± 1 nm) of the PMMA lamellar nanodomains initially present in the untreated sample form on the thin film surface. ZnO nanoparticles, capped with a mixture of *n*-hexadecylamine and *tert*-butylphosphonic acid, having an average diameter equal to ≈5.5 nm, were selectively included in the PS lamellar nanodomains of the PS-*b*- PMMA copolymer by dispersing the NPs and BCP in a common solvent (toluene) before thin films preparation. The successive UV-irradiation of the resultant nanocomposites, allowed an efficient PMMA removal and preservation of the initial morphology, adopting the same irradiation protocol identified for the neat BCP (nanocomposite first/nanopores after). CdSe nanoparticles, decorated with 3-mercaptopropionic acid, with a diameter of ≈3 nm were instead successfully included at the interface between the nanochannels and the PS lamellar domains by using dipping procedures, by simply exploiting the capillary force (nanopores first/nanocomposite after). The results of the present study confirm the high versatility of block-copolymers for the preparation of nanoporous templates with controlled morphology at nanoscale that can be used, for example, to organize nanoparticles onto solid supports. The dimensions, the morphology and the chemical characteristics of pores can be easily tuned by changing the blocks constituting the BCP, their molecular masses and the volume fraction. This possibility opens the opportunity to fabricate BCP-based nanoporous templates with tailored

properties for the inclusion a wide range of different nanoparticles depending on the final application of the nanocomposites.

Funding This research was carried out in the frame of STAR Program, financially supported by UniNA and Compagnia di San Paolo, and Ricerca di Ateneo Program (UniNa).

CRediT authorship contribution statement
Anna Malafronte: Conceptualization, Writing - review & editing, Methodology, Data curation, Formal analysis, Data analysis. **Alessandro Emendato:** Investigation, Methodology, Data curation, Formal analysis, Data analysis, Writing - original draft, preparation. **Finizia Auriemma:** Conceptualization, Writing - review & editing, Methodology, Data curation, Formal analysis, Data analysis. **Carmen Sasso:** Investigation, specifically performing the experiments to optimize the BCP morphology. **Michele Laus:** Methodology, Validation, Data curation, Formal analysis, Data Analysis. **Irdi Murataj:** Investigation, specifically performing the functionalization of the ITO supports with the random copolymers. **Federico Ferrarese Lupi:** Methodology, Validation, Data curation, Formal analysis, Data Analysis. **Claudio De Rosa:** Validation, Resources, Visualization.

Declaration of competing interest The authors declare that they have no known competing financial interests or personal relationships that could have appeared to influence the work reported in this paper.

Appendix A. Supplementary data Supplementary data to this article can be found online at https://doi. org/10.1016/j.polymer.2020.122983.

References

[1] F.S. Bates, G.H. Fredrickson, Block copolymer thermodynamics: theory and experiment, Annu. Rev. Phys. Chem. 41 (1990) 525, https://doi.org/10.1146/annurev.pc.41.100190.002521.
[2] I.W. Hamley, The Physics of Block Copolymers, Oxford University Press, Oxford, 1998.
[3] C.M. Bates, M.J. Maher, D.W. Janes, C.J. Ellison, C.G. Willson, Block copolymer lithography, Macromolecules 47 (2014) 2, https://doi.org/10.1021/ma401762n.
[4] J. Bang, U. Jeong, D.Y. Ryu, T.P. Russell, C.J. Hawker, Block copolymer nanolithography: translation of molecular level control to nanoscale patterns, Adv. Mater. 21 (2009) 4769, https://doi.org/10.1002/adma.200803302.
[5] K. Koo, H. Ahn, S.W. Kim, D.Y. Ryu, T.P. Russell, Directed self-assembly of block copolymers in the extreme: guiding microdomains from the small to the large, Soft Matter 9 (2013) 9059, https://doi.org/10.1039/C3SM51083B.
[6] S.B. Darling, Directing the self-assembly of block copolymers, Prog. Polym. Sci. 32 (2007) 1152, https://doi.org/10.1016/j.progpolymsci.2007.05.004.
[7] M. Park, C.K. Harrison, P.M. Chaikin, R.A. Register, D.H. Adamson, Block copolymer lithography: periodic arrays of ~1011 holes in 1 square centimeter, Science 276 (1997) 1401, https://doi.org/10.1126/science.276.5317.1401.
[8] P.M. Mansky, E.L. Chaikin, J. Thomas, Monolayer films of diblock copolymer microdomains for nanolithographic applications, Mater. Sci. 30 (1995) 1987, https://doi.org/10.1007/BF00353023.
[9] C. Park, J. Yoon, E.L. Thomas, Enabling nanotechnology with self assembled block copolymer patterns, Polymer 44 (2003) 6725, https://doi.org/10.1016/j.polymer.2003.08.011.
[10] S. F¨orster, M. Konrad, From self-organizing polymers to nano- and biomaterials, J. Mater. Chem. 13 (2003) 2671, https://doi.org/10.1039/B307512P.

[11] C. De Rosa, F. Auriemma, A. Malafronte, R. Di Girolamo, M. Lazzari, M. Nieto- Suarez, D. Hermida-Merino, I.W. Hamley, G. Portale, Tuning ordered pattern of Pd species through controlled block copolymer self-assembly, J. Phys. Chem. B 120 (2016) 6829, https://doi.org/10.1021/acs.jpcb.6b04380.
[12] C. De Rosa, R. Di Girolamo, F. Auriemma, G. Talarico, A. Malafronte, C. Scarica, M. Scoti, Controlling size and orientation of lamellar microdomains in crystalline block copolymers, ACS Appl. Mater. Interfaces 9 (2017) 31252, https://doi.org/10.1021/acsami.6b15913.
[13] S.P. Nunes, Block copolymer membranes for aqueous solution applications, Macromolecules 49 (2016) 2905, https://doi.org/10.1021/acs.macromol.5b02579.
[14] M. Martina, D.W. Hutmatcher, Biodegradable polymers applied in tissue engineering research: a review, Polym. Int. 56 (2007) 145, https://doi.org/10.1002/pi.2108.
[15] P. Samaddar, A. Deep, K.-H. Kim, An engineering insight into block copolymer self-assembly: contemporary application from biomedical research to nanotechnology, Chem. Eng. J. 342 (2018) 71, https://doi.org/10.1016/j.cej.2018.01.062.
[16] A.M. Urbas, M. Maldovan, P. DeRege, E.L. Thomas, Bicontinuous cubic block copolymer photonic crystals, Adv. Mater. 14 (2002) 1850, https://doi.org/10.1002/adma.200290018.
[17] M. Stefik, S. Guldin, S. Vignolini, U. Wiesner, U. Steiner, Block copolymer self-assembly for nanophotonics, Chem. Soc. Rev. 44 (2015) 5076, https://doi.org/10.1039/C4CS00517A.
[18] G. Zito, G. Rusciano, G. Pesce, A. Malafronte, R. Di Girolamo, G. Ausanio, A. Vecchione, A. Sasso, Nanoscale engineering of two-dimensional disordered hyperuniform block-copolymer assemblies, Phys. Rev. E. 92 (2015), https://doi.org/10.1103/PhysRevE.92.050601,050601.
[19] C. De Rosa, F. Auriemma, R. Di Girolamo, G. Piero Pepe, T. Napolitano, R. Scaldaferri, Enabling strategies in organic electronics using ordered block copolymer nanostructures, Adv. Mater. 22 (2010) 5414, https://doi.org/10.1002/adma.201002649.
[20] H.-Y. Hsueh, C.-T. Yao, R.-M. Ho, Well-ordered nanohybrids and nanoporous materials from gyroid block copolymer templates, Chem. Soc. Rev. 44 (2015) 1974, https://doi.org/10.1039/C4CS00424H.
[21] W.J. Cho, Y. Kim, J.K. Kim, Ultrahigh-Density array of silver nanoclusters for SERS substrate with high sensitivity and excellent reproducibility, ACS Nano 6 (2012) 249, https://doi.org/10.1021/nn2035236.
[22] F.L. Yap, P. Thoniyot, S. Krishnan, S. Krishnamoorthy, Nanoparticle cluster Arrays for high-performance SERS through directed self-assembly on flat substrates and on optical fibers, ACS Nano 6 (2012) 2056, https://doi.org/10.1021/nn203661n.
[23] C. De Rosa, F. Auriemma, C. Diletto, R. Di Girolamo, A. Malafronte, P. Morvillo, G. Zito, G. Rusciano, G. Pesce, A. Sasso, Toward hyperuniform disordered plasmonic nanostructures for reproducible surface-enhanced Raman spectroscopy, Phys. Chem. Chem. Phys. 17 (2015) 8061, https://doi.org/10.1039/C4CP06024E.
[24] M.R. Bockstaller, R.A. Mickiewicz, E.L. Thomas, Block copolymer nanocomposites: perspectives for tailored functional materials, Adv. Mater. 17 (2005) 1331, https://doi.org/10.1002/adma.200500167.
[25] G. Zito, G. Rusciano, A. Vecchione, G. Pesce, R. Di Girolamo, A. Malafronte, A. Sasso, Nanometal skin of plasmonic heterostructures for highly efficient near-field scattering probes, Sci. Rep. 6 (31113) (2016), https://doi.org/10.1038/srep31113.
[26] A. Haryono, W.H. Binder, Controlled arrangement of nanoparticle arrays in block-copolymer domains, Small 2 (2006) 600, https://doi.org/10.1002/smll.200500474.
[27] A. Malafronte, F. Auriemma, R. Di Girolamo, C. Sasso, C. Diletto, A. Di Mauro, E. Fanizza, P. Morvillo, A. Rodriguez, A. Munoz-Garcia, M. Pavone, C. De Rosa, Confinement of semiconductor

ZnO nanoparticles in block copolymer nanostructure, J. Phys. Chem. C 121 (2017) 16617, https://doi.org/10.1021/acs.jpcc.7b05125.
[28] A. Malafronte, A. Capretti, G.P. Pepe, C. Forestiere, G. Miano, F. Auriemma, C. De Rosa, R. Di Girolamo, Simple theoretical considerations for block-copolymer-based plasmonic metamaterials, Macromol. Symp. 359 (2016) 72, https://doi.org/10.1002/masy.201400178.
[29] J. Kao, T. Xu, Nanoparticle assemblies in supramolecular nanocomposite thin films: concentration dependence, J. Am. Chem. Soc. 137 (2015) 6356. https://pubs.acs.org/doi/10.1021/jacs.5b02494.
[30] L. Peponi, A. Tercjak, J. Gutierrez, H. Stadler, L. Torre, J.M. Kenny, I. Mondragon, Self-assembling of SBS block copolymers as templates for conductive silver nanocomposites, Macromol. Mater. Eng. 293 (2008) 568, https://doi.org/10.1002/mame.200800033.
[31] I. Barandiaran, J. Gutierrez, A. Tercjak, G. Kortaberria, Thin film nanocomposites based on SBM triblock copolymer and silver nanoparticles: morphological and dielectric analysis, Macromol. Mater. Eng. 302 (2017), https://doi.org/10.1002/mame.201700169,1700169.
[32] J. Gutierrez, A. Tercjak, I. Mondragon, Conductive behavior of high TiO2 nanoparticle content of inorganic/organic nanostructured composites, J. Am. Chem. Soc. 132 (2010) 873, https://doi.org/10.1021/ja908359k.
[33] J. Gutierrez, A. Tercjak, I. Garcia, I. Mondragon, The effect of thermal and vapor annealing treatments on the self-assembly of TiO2/PS-b-PMMA nanocomposites generated via the sol-gel process, Nanotechnology 20 (2009) 22560, https://doi.org/10.1088/0957-4484/20/22/225603.
[34] Q. Zhang, L. Zhang, J. Lin, Percolating behavior of nanoparticles in block copolymer host: hybrid particle-field simulations, J. Phys. Chem. C 121 (2017) 23705. https://pubs.acs.org/doi/10.1021/acs.jpcc.7b07337.
[35] J. Gu, R. Zhang, L. Zhang, J. Lin, Harnessing zone annealing to Program directional motion of nanoparticles in diblock copolymers: creating periodically well-ordered nanocomposites, Macromolecules 53 (2020) 2111, https://doi.org/10.1021/acs.macromol.0c00101.
[36] M.A. Hillmyer, Nanoporous materials from block copolymer precursors, Adv. Polym. Sci. 190 (2005) 137, https://doi.org/10.1007/12_002.
[37] T. Thurn-Albrecht, J. Schotter, G.A. Kastle, N. Emley, T. Shibauchi, L. Krusin- Elbaum, K. Guarini, C.T. Black, M.T. Tuominen, T.P. Russell, Ultrahigh-density nanowire arrays grown in self-assembled diblock copolymer templates, Science 290 (2000) 2126, https://doi.org/10.1126/science.290.5499.2126.
[38] J. Park, J. Yoon, M. Ree, S.K. Jang, J.K. Kim, Virus filtration membranes prepared from nanoporous block copolymers with good dimensional stability under high pressures and excellent solvent resistance, Adv. Funct. Mater. 18 (2008) 1371, https://doi.org/10.1002/adfm.200700832.
[39] H.Y. Hsueh, Y.C. Huang, R.M. Ho, C.H. Lai, T. Makida, H. Hasegawa, Nanoporous gyroid nickel from block copolymer templates via electroless plating, Adv. Mater. 23 (2011) 3041, https://doi.org/10.1002/adma.201100883.
[40] F. Auriemma, C. De Rosa, A. Malafronte, R. Di Girolamo, C. Santillo, Y. Gerelli, G. Fragneto, R. Barker, V. Pavone, O. Maglio, A. Lombardi, Nano-in-nano approach for enzyme immobilization based on block copolymers, ACS Appl. Mater. Interfaces 9 (2017) 29318, https://doi.org/10.1021/acsami.7b08959.
[41] A. Malafronte, F. Auriemma, C. Santillo, R. Di Girolamo, R. Barker, Y. Gerelli, C. De Rosa, Block copolymers-based nanoporous thin films with tailored morphology for biomolecules adsorption, Adv. Mater. Interfaces 7 (1901580) (2020), https://doi.org/10.1002/admi.201901580.
[42] S.A. Bhakta, T.E. Benavidez, C.D. Garcia, Immobilization of glucose oxidase to nanostructured films of polystyrene-block-poly(2-vinylpyridine), J. Colloid Interface Sci. 430 (2014) 351, https://doi.org/10.1016/j.jcis.2014.05.067.

[43] S.I. Kuzina, A.I. Mikhailov, Photo-oxidation of polymers 4. The dual mechanism of polystyrene photo-oxidation: a hydroperoxide and a photochain one, Eur. Polym. J. 37 (2001) 2319, https://doi.org/10.1016/S0014-3057(01)00028-3.
[44] M. Palacios, O. García, J. Rodríguez-Hern´andez, Constructing robust and functional micropatterns on polystyrene surfaces by using deep UV irradiation, Langmuir 29 (2013) 2756, https://doi.org/10.1021/la304931x.
[45] Q. Zhang, T. Xu, D. Butterfield, M.J. Misner, D. Yoel Ryu, T. Emrick, T. P Russell, Controlled placement of CdSe nanoparticles in diblock copolymer templates by electrophoretic deposition, Nano Lett. 5 (2005) 357, https://doi.org/10.1021/nl048103t.
[46] M.J. Misner, H. Skaff, T. Emrick, T.P. Russell, Directed deposition of nanoparticles using diblock copolymer templates, Adv. Mater. 15 (2003) 221, https://doi.org/10.1002/adma.200390050.
[47] H. Yokoyama, T.E. Mates, E.J. Kramer, Structure of asymmetric diblock copolymers in thin films, Macromolecules 33 (2000) 1888, https://doi.org/10.1021/ma9912047.
[48] T. Xu, C.J. Hawker, T.P. Russell, Interfacial interaction dependence of microdomain orientation in diblock copolymer thin films, Macromolecules 38 (2005) 2802, https://doi.org/10.1021/ma048005u.
[49] H.C. Kim, T.P. Russell, Ordering in thin films of asymmetric diblock copolymers, J. Polym. Sci., Part B: Polym. Phys. 39 (2001) 663, https://doi.org/10.1002/1099-0488(20010315)39:6<663::AID-POLB1040>3.0.CO;2-K.
[50] D.Y. Ryu, K. Shin, E. Drockenmuller, C.J. Hawker, T.P. Russell, A generalized approach to the modification of solid surfaces, Science 308 (2005) 236, https://doi.org/10.1126/science.1106604.
[51] P. Mansky, Y. Liu, E. Huang, T.P. Russell, C. Hawker, Controlling polymer-surface interactions with random copolymer brushes, Science 275 (1997) 1458, https://doi.org/10.1126/science.275.5305.1458.
[52] C. Sinturel, M. Vayer, M. Morris, M. Hillmyer, Solvent vapor annealing of block polymer thin films, Macromolecules 46 (2013) 5399, https://doi.org/10.1021/ma400735a.
[53] C. Jin, B.C. Olsen, E.J. Luber, J.M. Buriak, Nanopatterning via solvent vapor annealing of block copolymer thin films, Chem. Mater. 29 (2017) 176, https://doi.org/10.1021/acs.chemmater.6b02967.
[54] S. Xiong, L. Wan, Y. Ishida, Y.A. Chapuis, G.S.W. Craig, R. Ruiz, P.F. Nealey, Directed self-assembly of triblock copolymer on chemical patterns for sub-10-nm nanofabrication via solvent annealing, ACS Nano 10 (2016) 7855, https://doi.org/10.1021/acsnano.6b03667.
[55] F. Ferrarese Lupi, T.J. Giammaria, M. Ceresoli, G. Seguini, K. Sparnacci, D. Antonioli, V. Gianotti, M. Laus, M. Perego, Rapid thermal processing of self-assembling block copolymer thin films, Nanotechnology 24 (2013), 315601, https://doi.org/10.1088/0957-4484/24/31/315601.
[56] F. Ferrarese Lupi, T. J Giammaria, G. Seguini, M. Ceresoli, M. Perego, D. Antonioli, V. Gianotti, K. Sparnacci, M. Laus, Flash grafting of functional random copolymers for surface neutralization, J. Mater. Chem. C 2 (2014) 4909, https://doi.org/10.1039/C4TC00328D.
[57] K. Sparnacci, D. Antonioli, V. Gianotti, M. Laus, F. Ferrarese Lupi, T.J. Giammaria, G. Seguini, M. Perego, Ultrathin random copolymer-grafted layers for block copolymer self-assembly, ACS Appl. Mater. Interfaces 7 (2015) 10944, https://doi.org/10.1021/acsami.5b02201.
[58] K. Ellmer, Past achievements and future challenges in the development of optically transparent electrodes, Nat. Photon. 6 (2012) 809, https://doi.org/10.1038/nphoton.2012.282.
[59] C. Diletto, P. Morvillo, R. Di Girolamo, F. Auriemma, C. De Rosa, Selective inclusion of chromophore molecules into poly(styrene-b-methylmethacrylate) block copolymer nanodomains: a study of morphological, optical and electrical properties, J. Sol. Gel Sci. Technol. 73 (2015) 634, https://doi.org/10.1007/s10971-014-3572-5.

[60] K. Sparnacci, D. Antonioli, M. Perego, T.J. Giammaria, G. Seguini, F. Ferrarese Lupi, G. Zuccheri, V. Gianotti, High temperature surface neutralization process with random copolymers for block copolymer self-assembly, Polym. Int. 66 (2016) 459, https://doi.org/10.1002/pi.5285.
[61] P.D. Cozzoli, M.L. Curri, A. Agostiano, G. Leo, M. Lomascolo, ZnO nanocrystals by a non-hydrolytic route: synthesis and characterization, J. Phys. Chem. B 107 (2003) 4756, https://doi.org/10.1021/jp027533+.
[62] M.N. Kalasad, M.K. Rabinal, B.G. Mulimani, Ambient synthesis and characterization of high-quality CdSe quantum dots by an aqueous route, Langmuir 25 (2009) 12729, https://doi.org/10.1021/la901798y.
[63] T. Thurn-Albrecht, R. Steiner, J. DeRouchey, C.M. Stafford, E. Huang, M. Bal, M. Tuominen, C.J. Hawker, T.P. Russell, Nanoscopic templates from oriented block copolymer films, Adv. Mater. 12 (2000) 787, https://doi.org/10.1002/(SICI)1521-4095(200006)12:11<787::AID-ADMA787>3.0.CO;2–1.
[64] N. Iancu, R. Sharma, D.K. Seo, Low-temperature synthetic method for size-controlled CdSe nanocrystals: utilization of boron selenide, Chem. Commun. 20 (2004) 2298, https://doi.org/10.1039/B408702J.
[65] H.S. Mansur, A.A.P. Mansur, CdSe quantum dots stabilized by carboxylic-functionalized PVA: synthesis and UV-vis spectroscopy characterization, Mater. Chem. Phys. 125 (2011) 709, https://doi.org/10.1016/j.matchemphys.2010.09.068.